

Isotopic investigation of the lattice dynamics in CuBr

J. Serrano, T. Ruf, F. Widulle, C. T. Lin, and M. Cardona

Max-Planck-Institut für Festkörperforschung, Heisenbergstr. 1, 70569 Stuttgart, Germany

(Received 20 November 2000; revised manuscript received 26 February 2001; published 20 June 2001)

We present a detailed investigation of the Raman spectra of isotopically tailored CuBr at low temperature. The transverse optic (TO) phonon of CuBr exhibits an almost perfect Lorentzian line shape, whereas the longitudinal optic (LO) phonon displays a complex broad structure. The change of the TO frequency with the variation of the isotope composition can be well described within the *virtual crystal approximation* (VCA), which corresponds to a $\omega \propto \mu^{-1/2}$ dependence on the reduced mass μ . Slight deviations from this general trend are attributed to anharmonic renormalization and agree semiquantitatively with results extracted from previous measurements of the temperature dependence of the Raman spectra. In the LO case, the broad structure is resolved into three separate features, *A*, *B*, and *C*. While *A* and *B* are rather broad, *C* is a narrow peak located at the high-energy side of the LO structure. Two different trends are observed when analyzing the evolution of the LO structure with isotope substitution: peak *B* shows a $\propto \mu^{-1/2}$ behavior, analogous to that of the TO phonon, whereas peaks *A* and *C* shift almost only with the copper mass. The LO line shape is explained in terms of the *Fermi resonance* (FR) model, i.e., an interaction between the LO mode and a combination band of two acoustic phonons. We have performed a shell model calculation, with parameters taken from inelastic neutron scattering measurements, in order to obtain the one- and two-phonon densities of states (DOS). This calculation yields Raman line shapes in remarkable agreement with the experimental observations.

DOI: 10.1103/PhysRevB.64.045201

PACS number(s): 71.38.-k, 63.20.Ry, 78.30.Fs, 78.30.Hv

I. INTRODUCTION

In the last decade considerable effort has been devoted to the study of the effects of isotope substitution on the electronic and vibrational properties of semiconductors. Many investigations have been concerned with elemental materials, i.e., diamond, Si, Ge, of which crystals of some technologically interesting isotopic modifications have been grown. For example, it is well known that one of the limiting factors of the thermal conductivity is, along with other kinds of defects, the mixture of isotopes in crystals grown out of natural elements possessing more than one stable isotope; a remarkable contribution occurs due to elastic scattering by the different isotopes of the constituent atoms of the material. In the case of diamond, ^{12}C -enriched crystals have a significantly larger thermal conductivity, especially at 80 K.¹ In silicon this conductivity has been reported recently to be enhanced by a factor of up to 6 (at 20 K) through enrichment of ^{28}Si with respect to the natural abundance.² Isotope substitution also results in a change of the lattice constant, as it has been reported for diamond,³ Si,⁴ and Ge.^{5,6} Another related effect is the modification of the electronic band gap due to the dependence of the electron-phonon interaction and the lattice constant on the average isotopic mass \bar{m} .^{7,8}

These effects are related to modifications of the lattice dynamics through isotope substitution. Hence, the investigation of isotopically modified samples is not only useful to develop new technologically interesting materials, but it also provides a way to separate isotope-disorder-related effects from anharmonic processes. From such studies one gains a better understanding of the phonon decay mechanisms and their influence on many physical properties (e.g., phonon-phonon interaction, electron-phonon interaction, lattice parameters, thermal conductivity).⁹ In elemental semiconduc-

tors, the mass dependence of the phonon frequencies is simply given by $\bar{m}^{-1/2}$ in the harmonic approximation, independently of the phonon wave vector \mathbf{q} . This relation does not hold for binary compounds, where the changes of the phonon frequencies and atomic displacements (eigenvectors) with the mass of the constituent atoms are specific to each phonon branch j and wave vector \mathbf{q} .¹⁰ The different behavior of acoustic and optic branches by substitution of either heavy or light atoms allows one to probe the efficiency of the different anharmonic decay channels of Γ -point optical phonons (and, in principle, also of other phonons using spectroscopic techniques, such as inelastic neutron or x-ray scattering,¹¹ which allow one to probe larger wave vectors \mathbf{q}). In the case of GaP a double-peak structure has been recently reported for the Raman spectrum of the transverse optic (TO) phonons. Changes of the relative positions and intensities of the two peak components with Ga isotope substitution confirmed the anharmonic nature of this structure.^{12,13} This feature was also reproduced by first-principles calculations in which the anharmonicity was treated by density functional perturbation theory (DFPT).¹⁴

Isotope substitution and Raman scattering have been also used to determine phonon *eigenvectors* at the Brillouin zone center in cases where they are not fixed by symmetry, such as for the E_2 phonons of the wurtzite structure compounds CdS and GaN.^{15,16} In the case of SiC, the use of different polytypes allowed the investigation of the eigenvectors for nonzero \mathbf{q} along the Γ - L direction in the zinc-blende crystal structure.¹⁷ The measurement of phonon eigenvectors provides an important check for lattice-dynamical model calculations, since even an excellent fit of a given model only to measured *frequency* dispersion curves does not imply the reliability of the calculated *eigenvectors*. Moreover, many physical properties, such as inelastic neutron or light scatter-

ing intensities and selection rules, require a precise knowledge of the eigenvectors which, unfortunately, have received much less attention than the phonon frequencies.

Copper bromide, together with CuCl and CuI, is one of the most ionic materials with the zinc-blende structure at ambient conditions.^{18,19} Many of its physical properties are similar to those of CuCl, i.e., it displays a negative thermal expansion coefficient below 50 K,^{20–23} a relatively large ionic conductivity at high temperatures,^{24,25} and an anomalous increase of the band gap with increasing temperature.²⁶ X-ray absorption and neutron diffraction measurements show an increasing disorder of the Cu⁺ sublattice with increasing temperature,^{27–30} related to a large anharmonicity of its vibrational potentials. The largest anharmonic vibrational amplitudes are along the $\langle 111 \rangle$ direction.²⁸ The strong anharmonicity requires consideration of at least quartic terms in the interatomic potential expansion in order to describe properly many physical properties,^{27,29,30} and leads to a decrease of the Cu-Br bond length with increasing temperature above 300 K.³¹ The Raman spectrum of CuCl exhibits an anomalously broad structure in the TO region, consisting of three main peaks instead of the single-TO-phonon peak expected for zinc-blende compounds.³² Two different models have been applied to explain this unusual feature: In the so-called *off-center model*, one considers a disordered Cu⁺ sublattice with Cu⁺ ions displaced away from their tetrahedral positions due to off-center minima of the lattice potential. This leads to two different “TO modes” associated with two possible equilibrium positions for the Cu⁺ ions (the standard and the displaced positions).^{33–35} In the *Fermi resonance model*, one considers an anharmonic renormalization of the TO(Γ) phonon due to interactions with a two-phonon continuum of acoustic modes.^{36–40}

The Raman spectrum of CuBr at low temperature has been reported to show a TO(Γ) phonon with a normal Lorentzian line shape at ≈ 136 cm⁻¹, and a broad asymmetric peak at 169 cm⁻¹ corresponding to the *longitudinal optic* (LO) mode at the Γ point,^{41–43} with a linewidth of ≈ 7 cm⁻¹ at 6 K. When the temperature is increased, two new features arise around 70 cm⁻¹ and 125 cm⁻¹ at 246 K,⁴⁴ respectively. The first has been assigned to a 2TA combination, whereas the second structure was studied with the off-center and Fermi resonance models, either postulating a TO-phonon structure due to a double-well potential⁴⁵ (similar to that suggested by off-center models for CuCl) or using a TA+LA combination as an anharmonic decay channel of the TO(Γ) phonon⁴² (Fermi resonance model). Although none of these models seems to be conclusive in explaining *all* the available experimental data, there are some aspects that cannot be addressed by the off-center model, e.g., the changes of the Raman spectrum with isotope substitution in CuCl (Ref. 32) and the extended x-ray absorption fine structure measurements (EXAFS) in CuBr.²⁹

In this work we present a detailed investigation of the Raman spectrum of CuBr at 2 K with a set of isotopically tailored samples covering the four possible combinations of Cu and Br isotopes, in addition to those obtained from the natural elements. This study reveals the anharmonic nature of the LO(Γ) spectrum, which is resolved into three different

TABLE I. Isotope information for the investigated CuBr samples: isotopic composition, average mass \bar{m} , and mass variance parameter g . \bar{m} and g are obtained from the isotopic composition and the corresponding masses.

Isotope	Isotope content (%)	\bar{m} (amu)	g
⁶³ Cu	99.9 ^a	62.932	0.1×10^{-5}
^{nat} Cu	⁶³ Cu, 69.17; ⁶⁵ Cu, 30.83	63.546	21.1×10^{-5}
⁶⁵ Cu	99.7 ^a	64.922	0.3×10^{-5}
⁷⁹ Br	99.41 ^a	78.930	0.4×10^{-5}
^{nat} Br	⁷⁹ Br, 50.69; ⁸¹ Br, 49.31	79.904	15.6×10^{-5}
⁸¹ Br	98.75 ^a	80.891	0.8×10^{-5}

^aThe isotope content is the enrichment of the nominal isotope. The concentration of the other isotope is the difference between that value and 100%. The concentration of the most common impurities of other atoms was less than 300 ppm.

structures consisting of two overlapping broad features in the range ≈ 160 – 170 cm⁻¹, with a sharp peak at its high-energy side, around ≈ 172 cm⁻¹ for the natural sample. The line shape of this phonon is explained quantitatively by the Fermi resonance model. The change of the phonon frequencies with isotope composition is also addressed for the TO(Γ) phonon, while in the case of the LO structure more information is required in order to explain the observed dominance of Cu displacements in the two-phonon density of states (DOS) in this region. The fact that the Fermi resonance occurs for the TO phonon in CuCl, whereas in CuBr it occurs for the LO phonon, can be qualitatively attributed to the increase in reduced mass associated with the increase in the halogen mass when going from CuCl to CuBr. This increase shifts the TO phonon away from the two-phonon resonance region while bringing the LO mode closer to it.

II. EXPERIMENTAL DETAILS

Natural copper and bromine contain two stable isotopes each (⁶³Cu, 69.17%; ⁶⁵Cu, 30.83%; ⁷⁹Br, 50.69%; and ⁸¹Br, 49.31%). The elements used to grow our samples were isotopically pure (>99%) except for ⁸¹Br, whose enrichment quality was slightly lower (98.75%). The actual purity of the different isotopes was measured by means of mass spectroscopic analysis; their isotope enrichment is shown in Table I. The samples were of two kinds: (i) very tiny platelets of ≈ 1 mm² surface area and thickness less than 100 μ m, and (ii) conic single crystals with a base diameter of 1–2 mm and a length of 3–5 mm. The Raman spectra from both types of samples coincide for identical isotope composition. The growth method for samples of type (i) was the same used for growing the CuCl isotope-enriched crystals measured in Ref. 32; this method is described in Ref. 46, and allows one to grow small crystals reducing the amount of expensive isotope-enriched elements needed. Source materials for the growth of the CuBr isotopic mixed crystals were obtained by the chemical reaction of NaBr, Na⁷⁹Br, Na⁸¹Br, and CuSO₄·5H₂O, ⁶³CuSO₄·5H₂O, and ⁶⁵CuSO₄·5H₂O. Prior to this reaction, the sulfate was prepared by dissolving natural

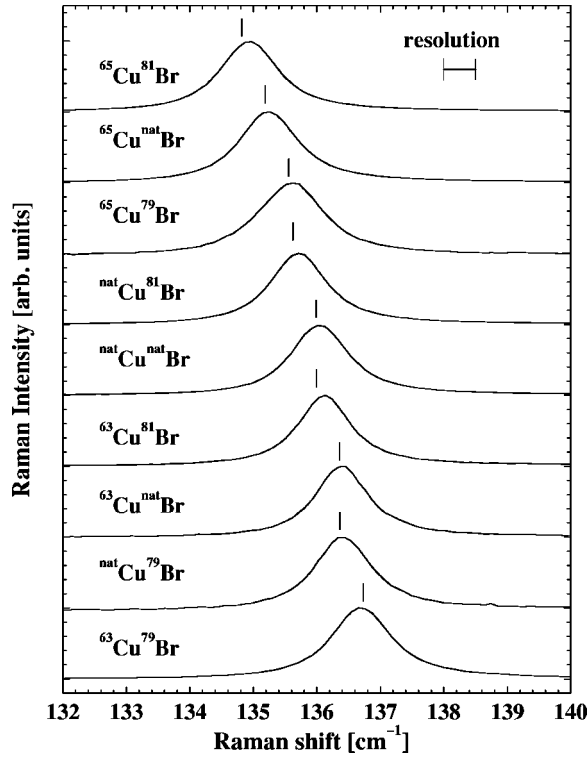


FIG. 1. Raman spectra of the TO(Γ) phonon of CuBr for different isotopically tailored samples. The vertical bars indicate the peak positions obtained from the harmonic virtual crystal approximation, which shift with $\mu^{-1/2}$.

or isotopic alloy enriched copper metal in diluted H_2SO_4 .³² CuBr conic single crystals of type (ii) were grown by sublimation of the CuBr powders in closed evacuated ampoules.

The Raman spectra were obtained using a triple-grating Dilor XY spectrometer operating in the high-dispersion mode. The scattered light was collected with a charge-coupled-device detector (CCD) cooled by liquid nitrogen. The 6470.9 Å Kr^+ line was used for excitation from a Kr-Ar mixed gas laser. The samples were immersed in superfluid helium and kept at temperatures below 2 K in an optical cryostat and measured in backscattering geometry. The laser power was adjusted between 25 and 50 mW to avoid sample heating. No changes in the spectra were observed when increasing the power by a factor of 2. The $^{65}\text{Cu}^{79}\text{Br}$ sample was so small that it had to be measured using a micro-Raman setup with a cold finger at 6 K under vacuum. The laser power was 28 mW and a $50\times$ objective was used in this case. The spectral resolution in both setups was $\approx 0.5 \text{ cm}^{-1}$. The 6532.9 Å line of a Ne lamp was used for calibration.

III. RESULTS

A. TO(Γ) phonon

Figure 1 displays the Raman spectra of CuBr in the region of the TO(Γ) phonon for different isotopic compositions. The intensities (peak height) are normalized and the spectra are ordered with increasing reduced mass from the bottom to the top. As the reduced mass, μ , increases, the phonon frequency decreases proportionally to $\mu^{-1/2}$.

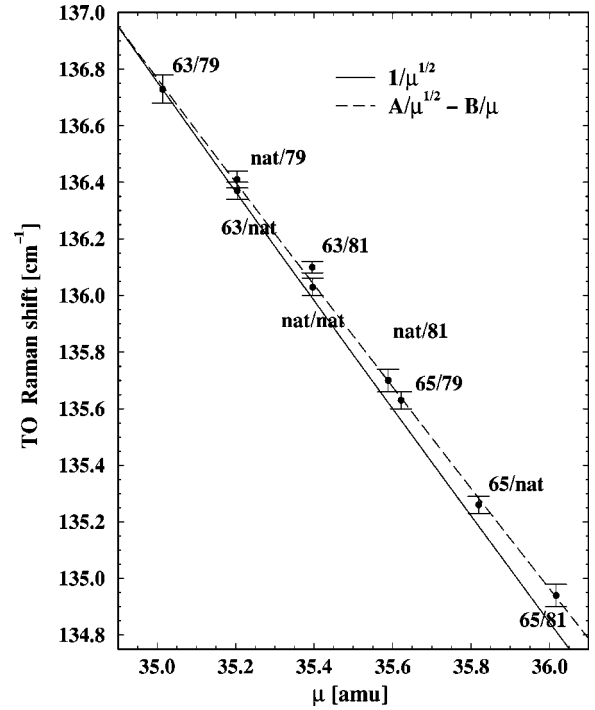


FIG. 2. Raman shift of the different CuBr samples vs the reduced mass μ . The solid line represents the $\propto \mu^{-1/2}$ behavior, using the $^{65}\text{Cu}^{79}\text{Br}$ TO frequency as reference. The dashed line represents a fit with Eq. (7) (see Sec. V).

For elemental crystals the virtual crystal approximation⁹ (VCA) predicts that all phonons should exhibit the same dependence ($\bar{m}^{-1/2}$) on the average isotopic mass \bar{m} in the harmonic approximation, independent of wave vector and branch. The extension to binary compounds is straightforward, but the dependence of the phonon frequency on the mass varies now with \mathbf{q} . In the case of the zone-center optic phonons in the zinc-blende structure, this relation holds for the reduced mass, i.e., $\omega_{\text{O}}(\Gamma) \propto \mu^{-1/2}$, where the subscript stands for optic modes.

The vertical bars in Fig. 1 illustrate this $\mu^{-1/2}$ scaling, with the phonon energy of the $^{63}\text{Cu}^{79}\text{Br}$ sample used as a reference. With increasing μ the measured TO(Γ) peak is shifted slightly towards higher frequencies than expected on the basis of the VCA. This difference reaches its maximum for $^{65}\text{Cu}^{81}\text{Br}$, with the experimental frequency $\approx 0.13(9) \text{ cm}^{-1}$ higher than the harmonic VCA prediction.

This deviation is also visible in Fig. 2, where the TO(Γ) frequency is shown as a function of the reduced mass. The error bars indicate the standard deviation determined from different measurements. The solid line represents the reduced mass behavior $\propto \mu^{-1/2}$ with respect to the $^{65}\text{Cu}^{79}\text{Br}$ sample. The reasons for this shift will be discussed in Sec. V.

The experimental TO(Γ) frequencies and the full width at half maximum (FWHM), $\Gamma_{\text{TO}(\Gamma)}$, for the different isotopic compositions are shown in Table II. $\Gamma_{\text{TO}(\Gamma)}$ was obtained by fitting the spectra with a Voigt profile (i.e., a convolution of a Gaussian and a Lorentzian), which implies a Lorentzian line shape for the phonon. This is justified by the excellent resolution achieved in the experiment and the almost sym-

TABLE II. Reduced mass μ , Raman frequencies $\omega_{\text{TO}(\Gamma)}$, $\omega_{\text{LO}(A)}$, $\omega_{\text{LO}(B)}$, and $\omega_{\text{LO}(C)}$, and linewidths $\Gamma_{\text{TO}(\Gamma)}$ (FWHM) of isotopically modified CuBr samples at $T=2$ K in units of cm^{-1} . The linewidth has been corrected for the spectrometer resolution by deconvolution with a Gaussian ($\Gamma_{\text{Gauss}} \approx 0.5 \text{ cm}^{-1}$). The error bars (in parentheses) are the standard deviation of several measurements.

Sample	μ (amu)	$\omega_{\text{TO}(\Gamma)}$	$\Gamma_{\text{TO}(\Gamma)}$	$\omega_{\text{LO}(A)}$	$\omega_{\text{LO}(B)}$	$\omega_{\text{LO}(C)}$
$^{63}\text{Cu}^{79}\text{Br}$	35.014	136.73(5)	0.90(2)	166.40(20)	168.35(20)	173.79(6)
$^{\text{nat}}\text{Cu}^{79}\text{Br}$	35.204	136.41(3)	0.81(1)	165.72(20)	168.22(20)	173.19(10)
$^{63}\text{Cu}^{\text{nat}}\text{Br}$	35.205	136.37(3)	0.79(1)	166.10(20)	168.10(20)	173.61(11)
$^{63}\text{Cu}^{81}\text{Br}$	35.395	136.10(2)	0.84(1)	165.97(20)	167.50(20)	173.42(8)
$^{\text{nat}}\text{Cu}^{\text{nat}}\text{Br}$	35.396	136.03(3)	0.87(1)	165.65(20)	167.50(20)	173.00(6)
$^{\text{nat}}\text{Cu}^{81}\text{Br}$	35.588	135.70(4)	0.85(3)	165.55(20)	167.10(20)	172.83(6)
$^{65}\text{Cu}^{79}\text{Br}^{\text{a}}$	35.622	135.63(3)	1.05(2)	164.20(25)	166.88(25)	171.51(8)
$^{65}\text{Cu}^{\text{nat}}\text{Br}$	35.819	135.26(3)	0.90(1)	164.40(20)	166.57(20)	171.43(5)
$^{65}\text{Cu}^{81}\text{Br}$	36.016	134.94(4)	0.86(1)	164.27(20)	166.13(20)	171.37(5)

^aData were taken at 6 K (see Sec. II).

metric line shape of these spectra.⁴⁷ Notice that the TO width changes very strongly with the bromine mass. $\Gamma_{\text{TO}(\Gamma)}$ increases by $\approx 7\%$ when going from $^{63}\text{Cu}^{81}\text{Br}$ to $^{63}\text{Cu}^{79}\text{Br}$, and by $\approx 22\%$ between $^{65}\text{Cu}^{81}\text{Br}$ and $^{65}\text{Cu}^{79}\text{Br}$. The different increments may be due to the different setup used to measure $^{65}\text{Cu}^{79}\text{Br}$ (see Sec. II). This variation with the bromine mass has the trend expected from anharmonic contributions; it is, however, much larger than that expected from the mass change, $\approx 2.5\%$.

B. LO(Γ) phonon

Figure 3 displays the Raman spectra of the LO(Γ) phonon for different isotopic compositions. Note that the spectra are now ordered with increasing copper mass from the bottom to the top. This phonon appears as a broad structure with a FWHM of around 17 cm^{-1} , showing three main features, labeled A, B, and C, located in natural CuBr around 166, 168, and 172 cm^{-1} , respectively. While features A and B are quite broad, C is an asymmetric and rather narrow peak located at the high-energy side of the LO(Γ)-phonon spectrum. The frequencies of these features are listed in Table II. The vertical bars in Fig. 3 indicate the frequencies that are expected for a $\mu^{-1/2}$ behavior with respect to the B peak of the $^{63}\text{Cu}^{79}\text{Br}$ sample. The most striking fact is that the mass dependence of B is quite different from that of A and C. The frequency shifts of the latter are mainly determined by the copper mass, whereas feature B follows the $\mu^{-1/2}$ behavior expected within the VCA for a zone-center optic phonon. The shift of the peak C observed when replacing ^{63}Cu by ^{65}Cu in the Cu^{81}Br sample amounts, for instance, to $\approx 2.05(13) \text{ cm}^{-1}$, which is much larger than the $\approx 1.50 \text{ cm}^{-1}$ anticipated from the reduced mass behavior.

Figure 4 shows the behavior of the three peak frequencies versus the reduced mass. The error bars correspond to the standard deviation of the results from several measurements. The maxima were found by analyzing the first derivative of the spectra, whose line shapes neither correspond to Lorentzians nor to Gaussians. The $\omega \propto \mu^{-1/2}$ behavior, taking $^{63}\text{Cu}^{79}\text{Br}$ as a reference, is displayed by the dashed lines. From these lines one notices that only feature B obeys the

expected $\propto \mu^{-1/2}$ behavior. The results for peaks A and C can be grouped into sets of samples with varying bromine but constant copper mass. Within each of these groups, denoted by \circ , \square , and \diamond in Fig. 4, the phonon frequency is almost independent of μ . However, the average mode frequency of each group roughly follows the $\mu^{-1/2}$ law. In other words, the A and C feature frequencies vary predominantly with the copper mass and are almost independent of the bromine mass.

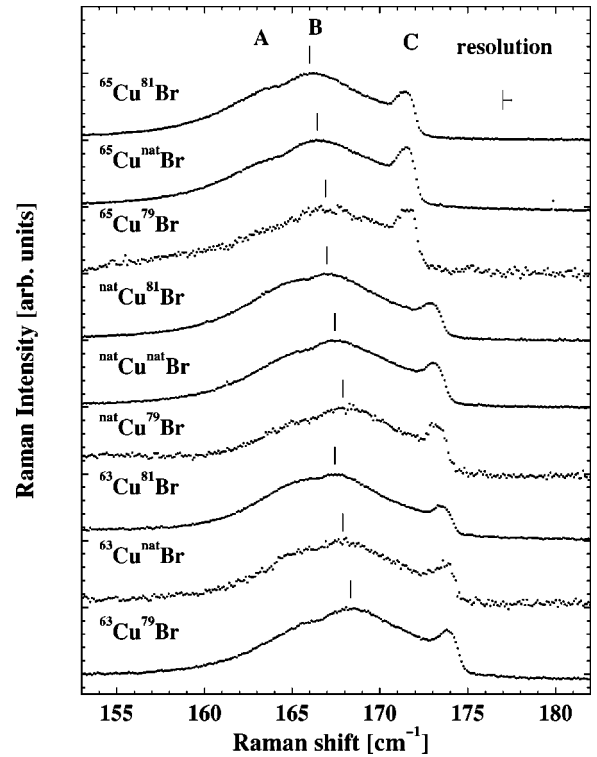


FIG. 3. Raman spectra of the CuBr LO(Γ) phonon at 2 K for different isotopic compositions. Three features can be clearly distinguished, two broad structures, labeled A and B, and a narrow peak at the high energy side, labeled C. The vertical bars indicate the peak positions obtained from the harmonic virtual crystal approximation, which shift with $\mu^{-1/2}$.

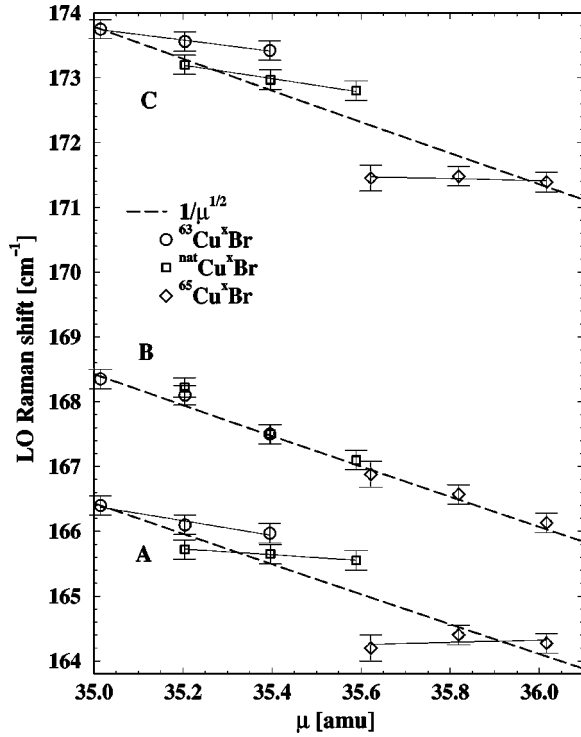


FIG. 4. Evolution of the Raman shift of the features A, B, and C of the LO(Γ) phonon in CuBr with the reduced mass. The dashed lines represent the $\mu^{-1/2}$ behavior of the harmonic VCA. The open circles, squares, and diamonds are experimental data for the $^{63}\text{Cu}^x\text{Br}$, $^{\text{nat}}\text{Cu}^x\text{Br}$, and $^{65}\text{Cu}^x\text{Br}$ samples, respectively. The solid lines represent linear fits to the A and C structures, separately for each sample set with the same copper isotope composition.

The different dependences exhibited by the frequencies of these three features are not specific to CuBr; similar effects have also been reported in the Raman studies of isotopically tailored GaP and CuCl in Refs. 12 and 32, respectively. In the case of CuCl, the TO phonon exhibits a broad structure with two main features, namely TO(γ) and TO(β), whose frequency shifts are proportional to changes of only the copper mass and the reduced mass, respectively, with varying isotopic composition. The fact that something similar appears in CuBr, this time, however, for the LO phonon, can be qualitatively understood as a change of the relative position of the one-phonon and two-phonon spectra with increasing halogen mass.⁴⁸ This will be further analyzed in Sec. V.

IV. THEORY

There are two different terms that contribute to the phonon frequency renormalization and linewidth: the inelastic anharmonic decay processes and elastic phonon scattering due to atomic disorder (isotopes and impurities).⁴⁹ Raman spectroscopy of isotopically tailored materials is a powerful technique to investigate this renormalization for zone-center phonons. It allows one to focus first on the study of isotopically pure samples, where only anharmonic self-energy processes are present, and then to turn to the more complex isotope mixtures, which show both kinds of effects simultaneously.

The renormalization of the phonon frequency and linewidth due to both, disorder-related effects and anharmonic decay, can be expressed by a self-energy

$$\Sigma(\mathbf{q}, j; \omega) = \Delta(\mathbf{q}, j; \omega) - \frac{i}{2} \Gamma(\mathbf{q}, j; \omega), \quad (1)$$

where $\Delta(\mathbf{q}, j; \omega)$ is the frequency shift of the phonon with frequency ω of branch j and wave vector \mathbf{q} , and $\Gamma(\mathbf{q}, j; \omega)$ represents its broadening (FWHM). To a first approximation we can treat both anharmonicity and disorder contributions in an additive way, i.e., $\Delta = \Delta_{\text{dis}} + \Delta_{\text{anh}}$ and $\Gamma = \Gamma_{\text{dis}} + \Gamma_{\text{anh}}$, where Δ and Γ are related by the Kramers-Kronig relations.⁵⁰ Therefore, we can use perturbation theory to address each term individually. If we confine ourselves to Raman spectroscopy with visible light, i.e., wave vector $\mathbf{q} \approx \mathbf{0}$, the spectral function of a particular phonon of frequency ω and branch j at low temperature is^{47,51}

$$A(\mathbf{0}, j; \omega) = \frac{1}{2\pi} \frac{\Gamma(\mathbf{0}, j; \omega)}{[\omega - \omega(\mathbf{0}, j) - \Delta(\mathbf{0}, j; \omega)]^2 + [\Gamma(\mathbf{0}, j; \omega)/2]^2}, \quad (2)$$

where $\omega(\mathbf{0}, j)$ represents the harmonic Raman frequency.

A. Disorder effects

Within second-order perturbation theory, isotope disorder can be characterized through a mass fluctuation parameter, $g(\kappa)$, for each atomic species κ :

$$g(\kappa) = \sum_i c_i \left[\frac{\bar{m}(\kappa) - m_i(\kappa)}{\bar{m}(\kappa)} \right]^2, \quad (3)$$

where c_i and m_i stand for the concentration and mass of isotope i , respectively, and $\bar{m}(\kappa)$ is the average mass of the atomic species κ , i.e., the sum of the isotope masses weighted by their respective concentrations. The actual values of $g(\kappa)$ for our CuBr samples are displayed in Table I. The highest values of $g(\kappa)$ are achieved, for the samples available, in the natural mixtures. However, since the maximum value of $g(\kappa)$ in CuBr is almost one order of magnitude smaller than that of $^{70}\text{Ge}_{0.5} \text{ } ^{76}\text{Ge}_{0.5}$, the most disordered Ge composition⁵² that has been reported to show an isotopic self-energy shift of $\approx 1 \text{ cm}^{-1}$, a very small effect is expected for CuBr. The contribution to the FWHM is then given by⁵³

$$\Gamma_{\text{dis}}(\mathbf{q}, j, \omega) = \frac{\pi}{6} \omega^2 \sum_{\kappa}^{\text{isot}} g(\kappa) |\mathbf{e}(\kappa|\mathbf{q}, j)|^2 \rho_{\kappa}^{(1)}(\omega), \quad (4)$$

where $\mathbf{e}(\kappa|\mathbf{q}, j)$ is the eigenvector of the phonon of branch j , wave vector \mathbf{q} , and atomic species κ , and $\rho_{\kappa}^{(1)}(\omega)$ the one-phonon partial density of states of the κ -atomic species. [The frequency shift $\Delta_{\text{dis}}(\omega)$ can be obtained from $\Gamma_{\text{dis}}(\omega)$ through the Kramers-Kronig relations.]

B. Anharmonic decay processes

Lattice-dynamical calculations are usually performed in the *harmonic approximation*, where the lattice potential is

expanded to quadratic terms in the atomic displacements only. However, in a real crystal the cubic and quartic terms in this expansion are often non-negligible. In this work we apply a simplified third-order perturbation approach to account for the anharmonic contribution to the phonon line-widths and frequencies. To this extent, the anharmonic broadening of the Raman line is given by⁵⁴

$$\Gamma_{\text{anh}}(\mathbf{0}, j; \omega) = \frac{18\pi}{\hbar^2} \sum_{\mathbf{q}, j_1, j_2} |V_3(\mathbf{0}, j; \mathbf{q}, j_1; -\mathbf{q}, j_2)|^2 \times [n(\mathbf{q}, j_1) + n(-\mathbf{q}, j_2) + 1] \delta(\omega(\mathbf{q}, j_1) + \omega(-\mathbf{q}, j_2) - \omega), \quad (5)$$

where $V_3(\mathbf{q}, j; \mathbf{q}_1, j_1; \mathbf{q}_2, j_2)$ are the cubic coefficients in the expansion of the lattice potential in normal coordinates, $n(\mathbf{q}, j)$ denotes the thermal occupation number of phonons of branch j and wave vector \mathbf{q} , and the δ distribution guarantees energy conservation. At low temperature the thermal occupation number vanishes and, assuming a constant value of the cubic coefficient independent of wave vector and branch, which, including the required prefactors, we label V_3 , Eq. (5) can be greatly simplified. The anharmonic contribution to the FWHM is then proportional to the two-phonon density of states, $\rho^{(2)}(\omega)$ (joint density of states approximation), which can be obtained from a variety of lattice-dynamical models,

$$\Gamma_{\text{anh}}(\mathbf{0}, j; \omega) = |V_3|^2 \rho^{(2)}(\omega). \quad (6)$$

The actual dependence of V_3 on ω is rather complicated,^{32,54} although there are a few first principles calculations available for some zinc-blende semiconductors.⁵⁵ The anharmonic phonon frequency shift, $\Delta_{\text{anh}}(\omega)$, can be obtained from the imaginary part of the corresponding self-energy, i.e., $\Gamma_{\text{anh}}(\omega)$, through the Kramers-Kronig transformation.

The anharmonic frequency renormalization can also be estimated from the temperature dependence of the phonon frequency. As described in Ref. 56, the phonon frequency at low temperature can be written as $\omega \approx A\bar{m}^{-1/2} - B\bar{m}^{-1}$ for a monatomic crystal. The factor $A\bar{m}^{-1/2}$ can be determined from the linear extrapolation to $T=0$ of the linear regime of the temperature-dependent Raman frequency, and the difference between this value and the actual frequency at $T=0$ corresponds to the term $B\bar{m}^{-1}$. Generalizing this expression for binary compounds, we can write for CuBr the anharmonically renormalized phonon frequency at low temperature as

$$\omega = A/\mu^{1/2} + C/m_{\text{Cu}} + D/m_{\text{Br}} + E/(m_{\text{Cu}}m_{\text{Br}})^{1/2}, \quad (7)$$

where the coefficients C , D , and E depend on the eigenvectors. Due to the relatively small difference between m_{Cu} and m_{Br} , a rough approximation consists of using the reduced mass instead of both masses, i.e., $m_{\text{Cu}} \approx m_{\text{Br}} \approx 2\mu$, recovering again the equation for elemental crystals in terms of the reduced mass.

V. DISCUSSION

As mentioned in Sec. III A, the TO-phonon frequency versus μ shows a small but significant uniform shift with respect to the harmonic VCA predictions. This deviation has to be attributed to anharmonic processes, since it occurs systematically in all samples, either isotopically pure or mixed. Following the arguments exposed in the previous section, we performed a fit of the experimental data to the equation $A\mu^{-1/2} - B\mu^{-1}$ (dashed line in Fig. 2), obtaining for the anharmonic renormalization $B\mu^{-1} \approx 7.6 \text{ cm}^{-1}$ for natural CuBr. This value is in rather good agreement with data derived from the temperature-dependent Raman frequencies reported in Refs. 41, 42, and 44, which imply a renormalization of about 5.4 and 6 cm^{-1} , respectively. In Fig. 2 we compare this fit to the experimental data, and show this systematic deviation from the $\mu^{-1/2}$ reduced mass behavior expected for harmonic crystal. The large value of this shift (compared to that of germanium $\approx 2 \text{ cm}^{-1}$ from Ref. 47) can be attributed to the anharmonicity of CuBr, which is related to its structural instability, being one of the few halides with zinc-blende crystal structure at ambient pressure and having a phase transition at $p \approx 4.9 \text{ GPa}$.⁵⁷ A better quantitative approach may require a detailed and reliable description of the eigenvectors throughout the whole phonon dispersion relations, beyond that which is presently available.

In the LO case, the most striking feature is at first sight its anomalous line shape, quite different from the Lorentzian-like peak that one would expect to encounter for a ‘‘normal’’ zone-center phonon.⁴⁷ In order to address the nature of this anomaly, we considered first the picture obtained from Raman investigations on CuCl where a very similar multifeature structure has been reported for the TO phonon (see Ref. 32 and references therein). In Ref. 32 a simple model based on an anharmonic coupling between the two-phonon density of states and the TO phonon allowed the description of the Raman spectra and their change with isotope substitution. The various features of the TO Raman spectra of CuCl were explained as a result of a number of singularities located near zeros of the denominator in Eq. (2). This is the so-called Fermi resonance model (FR).³⁶⁻⁴⁰ Several available lattice-dynamical models can be used to calculate the one- or two-phonon DOS.⁵⁸⁻⁶⁰ In Fig. 5(a) we display the phonon dispersion calculated with the 14-parameter shell model of Hoshino,⁵⁹ using the parameter set I (SM-I). Figure 5(b) shows the corresponding two-phonon DOS, and the inset displays the significant differences found between the DOS calculated from the shell model of Ref. 59 (with two different sets of parameters, i.e., SM-I and SM-II) and the rigid-ion model (RIM) of Plumelle *et al.*,⁶⁰ obtained by fitting the same inelastic neutron scattering data.⁵⁹ The RIM and the SM-I display a dip in the DOS around the LO(Γ) phonon frequency. This dip corresponds to a reduction of the LA+TA decay channels.

We have calculated the anharmonic renormalization of the LO-phonon line shape due to the Fermi resonance with the two-phonon DOS using the three sets of parameters described above; the best agreement with the experimental

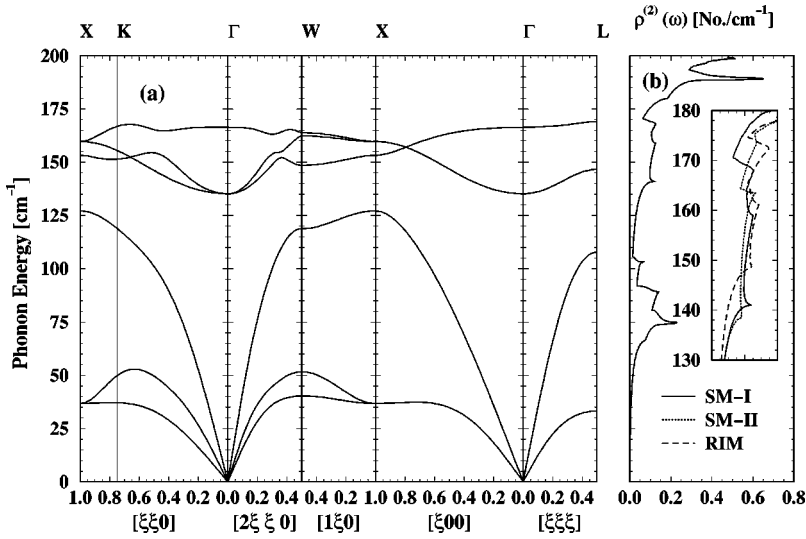


FIG. 5. (a) Phonon dispersion curves of CuBr calculated with the shell model along several high-symmetry directions. The parameters used are those of set I in Ref. 59. (b) Two-phonon DOS, $\rho^{(2)}(\omega)$, obtained with the same model. The inset represents an enlargement where the results of various models for $\rho^{(2)}(\omega)$ are compared in the frequency region of interest to the Fermi resonance under discussion (see Sec. V).

spectra was found for the parameter set SM-I. In Fig. 6(a) we display the real and imaginary parts of the anharmonic phonon self-energy defined in Eq. (1) and the Raman spectrum calculated with Eq. (2) for natural CuBr. As adjustable parameters we used the effective cubic coefficient V_3 defined in the previous section, and a rigid shift of the whole two-

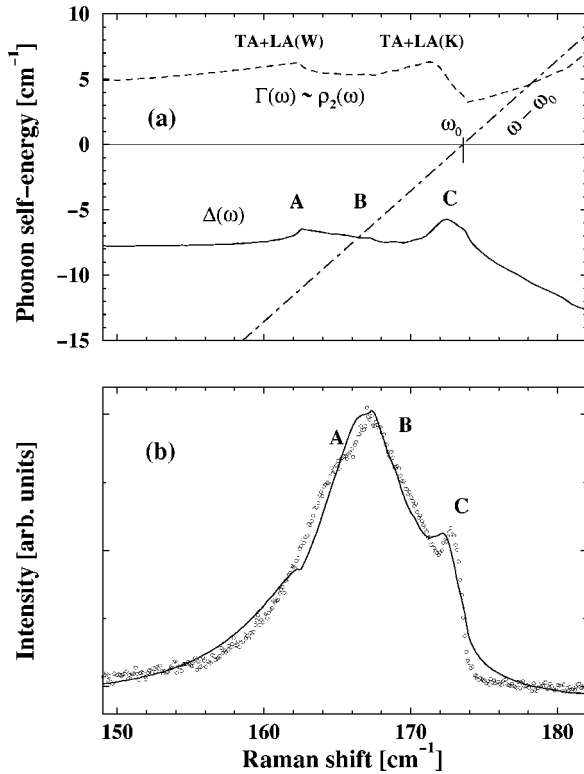


FIG. 6. (a) Imaginary part, $\Gamma(\omega)$, (dashed line) and real part, $\Delta(\omega)$, (solid line) of the phonon self-energy in natural CuBr calculated from Ref. 59 (see text). The dot-dashed line represents $(\omega - \omega_0)$, where ω_0 stands for the harmonic unrenormalized LO frequency. (b) Raman spectrum of the LO phonon of natural CuBr at 2 K (open circles). The three features (A, B, C) described in the text are shown together with a fit (solid line) using the FR model and the phonon self-energy of (a).

phonon DOS by about $\approx 3 \text{ cm}^{-1}$, which is well within the uncertainty of the neutron scattering measurements. A value of $|V_3|^2 \approx 45 \text{ cm}^{-2}$ yields remarkable agreement between the experimental line shape and the FR model calculations, as shown in Fig. 6(b). This value of $|V_3|^2$ is rather close to that used in Ref. 12 for similar calculations for GaP ($|V_3|^2 \approx 53 \text{ cm}^{-2}$). In Ref. 32, $|V_3|^2 \approx 70 \text{ cm}^{-2}$ was found to reproduce the TO-phonon line shape in CuCl. According to Eq. (2), the maxima in the Raman spectra correspond to minima in the denominator, i.e., to zeros or near-zeros of the expression $\omega - \omega(\mathbf{0}, j) - \Delta(\omega)$. We can see in Fig. 6(a) that there are two prominent features in the vicinity of the ‘‘harmonic’’ LO frequency at $\approx 166 \text{ cm}^{-1}$. These features correspond to the two-acoustic-phonon combination TA+LA at the W and K points, respectively. The small shoulder A, located at the low-energy side of the phonon structure, can therefore be attributed within this model to a (TA+LA)-phonon combination at the W point. The fact that there are no neutron data available for this point leaves us with a slight uncertainty in the actual position of the shoulder. The narrow peak at $\approx 172 \text{ cm}^{-1}$ then constitutes a resonance of the tail of the two-phonon DOS at frequencies higher than the TA+LA combination around the K point. Comparing this two-phonon DOS in the LO region with that used in Ref. 32 to explain the anomalous TO-phonon line shape in CuCl, we conclude that the physics behind both anomalies is basically the same. In fact, if we look at the two-phonon DOS calculated for CuCl in Ref. 32, the region at the TO(Γ)-phonon resembles remarkably the DOS in CuBr at the LO(Γ)-phonon frequency. The halogen substitution essentially leaves the acoustic DOS unchanged (it mostly depends on the copper mass) while the optic-mode zone-center frequencies are reduced according to $\propto \mu^{-1/2}$ between CuCl and CuBr. Hence the LO mode in CuBr and the TO mode in CuCl are close to the same two-phonon DOS feature (which has an acoustic-mode origin). This allows the FR model to explain both cases with the same arguments.

In Ref. 32 a narrow peak [labeled TO(γ)] was found, which exhibited mainly a dependence on the copper mass with isotope substitution. It was argued there that the domi-

nant copper displacements of the acoustic-phonon eigenvectors lead to a copper-mass dependence of the two-phonon DOS at the TO phonon frequency, explaining the changes of the Raman spectra with different isotopic composition. In the case of CuBr, we observe in Fig. 3 that the features A and C, attributed to Van Hove singularities of the DOS, vary also predominantly with the copper mass. One would, however, expect the behavior of the acoustic phonons to be determined mainly by the bromine mass, since bromine is the heavier of the two ions. Using $\Delta(\omega)$ and $\Gamma(\omega)$ from the above-mentioned lattice-dynamical models in the FR model, it was not possible to describe the isotope dependence of the LO structure. The masses of the copper and bromine ions are quite similar, which suggests that strong mixing of the eigenvectors may occur in the acoustic phonons. Therefore, a very precise knowledge of the atomic displacements is needed in order to obtain an accurate two-phonon DOS and the right description of its shift with the isotopic composition. A simple model, without taking into account these effects, cannot be expected to reproduce line shape changes due to such subtle effects. In the case of CuCl, however, there is a large difference between the anion and cation masses. This explains the excellent description of the isotope dependence of the Raman spectra of CuCl by the FR model. It has been demonstrated by X-ray measurements^{29,30} that the quartic-order anharmonic contribution is not negligible in CuBr but may be as important as the third-order term. This can lead also to a different isotope dependence of the phonon frequencies, without dramatic changes in the expected phonon line shape.⁵⁴

A simple argument can be used to infer possible anomalies in the eigenvectors: The relative difference between the LA(X) and LO(X) frequencies should be proportional to the square root of the ratio of the ion masses, provided that both modes have the same effective force constant, i.e., for CuCl, $\omega_{\text{LO}(X)}/\omega_{\text{LA}(X)} \approx (m_{\text{Cu}}/m_{\text{Cl}})^{1/2}$. If we use the values of Ref. 61, we obtain a frequency ratio of ≈ 1.9 whereas the mass ratio is 1.33; this leads to a force constant ratio $(k_{\text{Cl}}/k_{\text{Cu}})^{1/2} \approx 1.4$. An interpretation of this observation is that the LA(X) copperlike phonon in CuCl has a lower frequency, in addition to the mass effect, due to the smaller force constant associated with the copper-copper interaction. If we assume the same force constant ratio for CuBr and take the mass ratio $(m_{\text{Br}}/m_{\text{Cu}})^{1/2} \approx 1.12$, we can explain the observed frequency ratio of ≈ 1.21 by exchanging the mass dependence of the LA and LO phonons at the X point (see also Ref. 8, p. 15188). This is shown graphically in Fig. 7. *Ab initio* calculations of the phonon eigenvectors and the pressure dependence of the different decay channels are required to explain, in a quantitative way, the copper-mass dependence of the two-phonon DOS in the LO region inferred from our measurements.

Isotope disorder effects on the Raman phonons of CuBr are expected to be small because of the low values of both the mass variance parameters, $g(\kappa)$, and the corresponding partial one-phonon densities of states. At the TO-phonon frequency, the one-phonon DOS vanishes (see dispersion relations in Fig. 5). This leads to negligible contributions of elastic scattering by isotope disorder to the linewidth, as

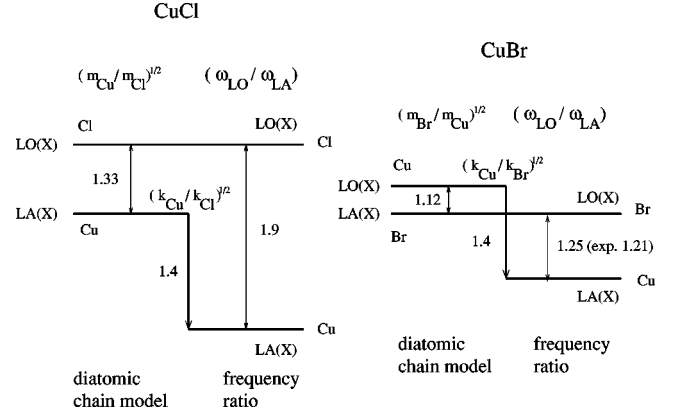


FIG. 7. Schematic explanation of the “copperlike” behavior of the acoustic-phonon DOS in CuBr. On the left side we display the change between the diatomic chain model prediction and the actual frequency ratio at the X point for CuCl obtained from inelastic neutron scattering, leading to a larger force constant for chlorine. On the right side of the figure, the same force constant ratio found in CuCl is assumed for CuBr. Together with the diatomic chain model predictions, this leads to a frequency ratio of ≈ 1.25 , in good agreement with the value of 1.21 obtained from the neutron data from Ref. 59. This argument holds provided that an exchange of the mass dependence between acoustic and optic phonons occurs, i.e., the acoustic modes shift with the lighter (copper) mass, and the optic ones shift with the heavier (bromine) mass.

expected from Eq. (4). However, the frequency renormalization Δ_{dis} results from an integral involving virtual transitions over the whole Brillouin zone, leading to a small but significant shift. This can be observed when comparing the TO-phonon frequencies of $^{63}\text{Cu}^{81}\text{Br}$ and natural CuBr. Within the error bars, the experimental disorder-related shift of $\approx -0.07(5) \text{ cm}^{-1}$ is in agreement with a value of -0.04 cm^{-1} obtained from Eq. (4) with the one-phonon DOS calculated using the SM-I of Ref. 59, assuming equal eigenvector components for copper and bromine. In the case of the LO phonon, the isotope disorder effects are completely masked by the strong anharmonic processes, which, as discussed earlier, alter the phonon line shape dramatically.

VI. CONCLUSIONS

We have investigated the Raman spectra of isotopically tailored CuBr. The TO phonon shows a normal Lorentzian-like line shape, which, to a first approximation, scales in frequency like $\mu^{-1/2}$ with isotope substitution. In contrast, for CuCl the TO phonons exhibit a strongly anomalous, non-Lorentzian, line shape. In addition, for CuBr the TO phonon it displays a slight deviation from the $\mu^{-1/2}$ behavior that can be attributed to anharmonic renormalization. We obtained an anharmonic shift of $\approx +7.6 \text{ cm}^{-1}$ for natural CuBr, in good agreement with the value of $\approx +5.5$ extrapolated from temperature-dependent Raman measurements. A small isotopic disorder effect is also observed in the TO-phonon frequency of natural CuBr. The LO phonon exhibits a complicated broad structure consisting of three features, similar to those observed for the TO phonons of CuCl, which can be explained by means of the Fermi resonance model. This work on CuBr provides strong

support for the anharmonic, Fermi resonance model, as opposed to the off-center models. Our isotope data reveal a copperlike behavior of the eigenvectors involved in the two-phonon acoustic DOS in this region. The microscopic origin of this effect is not completely understood. More work is needed in order to determine reliably the eigenvectors involved in the corresponding decay processes.

ACKNOWLEDGMENTS

We thank W. Kress for a critical reading of the manuscript. J.S. acknowledges support from Max-Planck-Gesellschaft and Ministerio de Educación y Ciencia (Spain) through the Plan Nacional de Formación del Personal Investigador.

- ¹J. R. Olsen, Phys. Rev. B **47**, 14 850 (1993).
- ²T. Ruf, R. W. Henn, M. Asen-Palmer, E. Gmelin, M. Cardona, H.-J. Pohl, G. G. Devyatych, and P. G. Sennikov, Solid State Commun. **115**, 243 (2000).
- ³H. Holloway, K. C. Hass, M. A. Tamor, T. R. Anthony, and W. R. Banholzer, Phys. Rev. B **44**, 7123 (1991).
- ⁴J. Zegenhagen *et al.*, in *Proceedings of the 25th International Conference on the Physics of Semiconductors, Osaka, 2000*, edited by N. Miura and T. Ando (Springer, Heidelberg, 2001), p. 125.
- ⁵R. C. Buschert, A. E. Merlini, S. Pace, S. Rodriguez, and M. H. Grimsditch, Phys. Rev. B **38**, 5219 (1988).
- ⁶A. Kazimirov, J. Zegenhagen, and M. Cardona, Science **282**, 930 (1998).
- ⁷N. Garro, A. Cantarero, M. Cardona, A. Göbel, T. Ruf, and K. Eberl, Phys. Rev. B **54**, 4732 (1996).
- ⁸A. Göbel, T. Ruf, M. Cardona, C. T. Lin, J. Wrzesinski, M. Steube, K. Reimann, J.-C. Merle, and M. Joucla, Phys. Rev. B **57**, 15 183 (1998).
- ⁹M. Cardona, in *Festkörperprobleme*, edited by R. Helbig, Vol. 34 of *Advances in Solid State Physics* (Vieweg, Braunschweig, 1994), p. 35.
- ¹⁰J. Menéndez, J. P. Page, and S. Guha, Philos. Mag. B **70**, 651 (1994).
- ¹¹T. Ruf, J. Serrano, M. Cardona, P. Pavone, M. Pabst, M. Krisch, M. D'Astuto, T. Suski, I. Grzegory, and M. Leszczynski, Phys. Rev. Lett. **86**, 906 (2001).
- ¹²F. Widulle, T. Ruf, A. Göbel, E. Schönherr, and M. Cardona, Phys. Rev. Lett. **82**, 5281 (1999).
- ¹³F. Widulle, T. Ruf, E. Schönherr, and M. Cardona, Phys. Status Solidi B **215**, 131 (1999).
- ¹⁴A. Debernardi, Solid State Commun. **113**, 1 (2000).
- ¹⁵J. M. Zhang, T. Ruf, A. Göbel, A. Debernardi, R. Lauck, and M. Cardona, in *Proceedings of the 23rd International Conference on the Physics of Semiconductors*, edited by M. Scheffler and R. Zimmermann (World Scientific, Singapore, 1996), p. 201.
- ¹⁶J. M. Zhang, T. Ruf, M. Cardona, O. Ambacher, M. Stutzmann, J.-M. Wagner, and F. Bechstedt, Phys. Rev. B **56**, 14 399 (1997).
- ¹⁷F. Widulle, T. Ruf, O. Buresch, A. Debernardi, and M. Cardona, Phys. Rev. Lett. **82**, 3089 (1999).
- ¹⁸J. C. Phillips, Rev. Mod. Phys. **42**, 317 (1970).
- ¹⁹L. Pauling, Phys. Today **24**(2), 9 (1971).
- ²⁰H. F. Schaake, Air Force Cambridge Research Laboratories, Report No. AFCRL-69-0538, 1969 (unpublished).
- ²¹C. Carabatos, B. Hennion, K. Kunc, F. Moussa, and C. Schwab, Phys. Rev. Lett. **26**, 770 (1971).
- ²²B. Hennion, F. Moussa, B. Prevot, C. Carabatos, and C. Schwab, Phys. Rev. Lett. **28**, 964 (1972).
- ²³J. N. Plendl and L. C. Mansur, Appl. Opt. **11**, 1194 (1972), and references therein.
- ²⁴J. B. Boyce, T. M. Hayes, and J. C. Mikelsen, Jr., Phys. Rev. B **23**, 2876 (1981).
- ²⁵S. Hull and D. A. Keen, J. Phys.: Condens. Matter **8**, 6191 (1996).
- ²⁶S. Lewonczuk, J. G. Gross, and J. Ringeisen, J. Phys. (France) Lett. **42**, L-91 (1981).
- ²⁷J. Harada, H. Suzuki, and S. Hoshino, J. Phys. Soc. Jpn. **41**, 1707 (1976).
- ²⁸V. M. Nield, R. L. McGreevy, D. A. Keen, and W. Hayes, Physica B **202**, 159 (1994).
- ²⁹J. M. Tranquada and R. Ingalls, Phys. Rev. B **28**, 3520 (1983).
- ³⁰F. Altorfer, B. Graneli, P. Fischer, and W. Bührer, J. Phys.: Condens. Matter **8**, 9949 (1994).
- ³¹M. Minicucci and A. Di Cicco, Phys. Rev. B **56**, 11 456 (1997).
- ³²A. Göbel, T. Ruf, C.-T. Lin, M. Cardona, J.-C. Merle, and M. Joucla, Phys. Rev. B **56**, 210 (1997), and references therein.
- ³³Z. Vardeny and O. Brafman, Phys. Rev. B **19**, 3276 (1979).
- ³⁴C. H. Park and D. J. Chadi, Phys. Rev. Lett. **76**, 2314 (1996).
- ³⁵S. R. Bickham, J. D. Kress, L. A. Collins, and R. Stumpf, Phys. Rev. Lett. **83**, 568 (1999).
- ³⁶J. Ruvalds and A. Zawadowski, Phys. Rev. B **2**, 1172 (1970).
- ³⁷M. Krauzmann, R. M. Pick, H. Poulet, G. Hamel, and B. Prevot, Phys. Rev. Lett. **33**, 528 (1974).
- ³⁸G. Kanellis, W. Kress, and H. Bilz, Phys. Rev. Lett. **56**, 938 (1986).
- ³⁹G. Kanellis, W. Kress, and H. Bilz, Phys. Rev. B **33**, 8724 (1986).
- ⁴⁰G. Kanellis, W. Kress, and H. Bilz, Phys. Rev. B **33**, 8733 (1986).
- ⁴¹J. E. Potts, R. C. Hanson, and C. T. Walker, Solid State Commun. **13**, 389 (1973).
- ⁴²T. Fukumoto, S. Nakashima, K. Tabuchi, and A. Mitsuishi, Phys. Status Solidi B **73**, 341 (1976).
- ⁴³H. D. Hochheimer, M. L. Shand, J. E. Potts, R. C. Hanson, and C. T. Walker, Phys. Rev. B **14**, 4630 (1976).
- ⁴⁴E. H. Turner, I. P. Kaminov, and C. Schwab, Phys. Rev. B **9**, 2524 (1974).
- ⁴⁵Z. Vardeny and O. Brafman, Phys. Rev. B **21**, 2585 (1980).
- ⁴⁶C. T. Lin, E. Schönherr, A. Schmeding, T. Ruf, A. Göbel, and M. Cardona, J. Cryst. Growth **167**, 612 (1996).
- ⁴⁷J. Menéndez and M. Cardona, Phys. Rev. B **29**, 2051 (1984).
- ⁴⁸T. Murahashi, T. Koda, Y. Oka, and T. Kushida, Solid State Commun. **13**, 307 (1973).
- ⁴⁹P. Etchegoin, H. D. Fuchs, J. Weber, M. Cardona, L. Pintschovius, N. Pyka, E. E. Haller, and K. Itoh, Phys. Rev. B **48**, 12 661 (1993).
- ⁵⁰P. Y. Yu and M. Cardona, *Fundamentals of Semiconductors* (Springer, Berlin, 1999), p. 239.

- ⁵¹M. Cardona and T. Ruf, *Solid State Commun.* **117**, 201 (2001).
- ⁵²J. M. Zhang, M. Gehler, A. Göbel, T. Ruf, M. Cardona, E. E. Haller, and K. Itoh, *Phys. Rev. B* **57**, 1348 (1998).
- ⁵³S. Tamura, *Phys. Rev. B* **30**, 849 (1984).
- ⁵⁴M. Balkanski, R. F. Wallis, and E. Haro, *Phys. Rev. B* **28**, 1928 (1983).
- ⁵⁵A. Debernardi, *Phys. Rev. B* **57**, 12 847 (1998).
- ⁵⁶D. T. Wang, A. Göbel, J. Zegenhagen, and M. Cardona, *Phys. Rev. B* **56**, 13 167 (1997).
- ⁵⁷S. Hull and D. A. Keen, *Phys. Rev. B* **50**, 5868 (1994).
- ⁵⁸B. Prevot, C. Carabatos, C. Schwab, B. Hennion, and F. Moussa, *Solid State Commun.* **113**, 1725 (1973).
- ⁵⁹S. Hoshino, *J. Phys. Soc. Jpn.* **41**, 965 (1976).
- ⁶⁰P. Plumelle, D. N. Talwar, M. Vandevyver, K. Kunc, and M. Zigone, *Phys. Rev. B* **20**, 4199 (1979).
- ⁶¹H. Bilz and W. Kress, *Phonon Dispersion Relations in Insulators*, edited by M. Cardona, P. Fulde, and H.-J. Queisser (Springer, Berlin, 1979), pp. 114 and 115.